PHYSOR 2012 – Advances in Reactor Physics – Linking Research, Industry, and Education
Knoxville, Tennessee, USA, April 15-20, 2012, on CD-ROM, American Nuclear Society, LaGrange Park, IL (2012)

THE METHOD OF CHARACTERISTICS FOR 2-D MULTIGROUP AND POINTWISE TRANSPORT CALCULATIONS IN SCALE/CENTRM

Kang Seog Kim and Mark L. Williams
Oak Ridge National Laboratory
One Bethel Valley Road, P.O. Box 2008, Oak Ridge, TN 37831-6172, USA
kimk1@ornl.gov; williamsml@ornl.gov

ABSTRACT

SCALE 6 computes problem-dependent multigroup (MG) cross sections through a combination of the conventional Bondarenko shielding-factor method and a deterministic pointwise (PW) transport calculation of the fine-structure spectra in the resolved resonance and thermal energy ranges. The PW calculation is performed by the CENTRM code using a 1-D cylindrical Wigner-Seitz model with the white boundary condition instead of the real rectangular cell shape to represent a lattice unit cell. The pointwise fluxes computed by CENTRM are not exact because a 1-D model is used for the transport calculation, which introduces discrepancies in the MG self-shielded cross sections, resulting in some deviation in the eigenvalue. In order to solve this problem, the method of characteristics (MOC) has been applied to enable the CENTRM PW transport calculation for a 2-D square pin cell. The computation results show that the new BONAMI/CENTRM-MOC procedure produces very precise self-shielded cross sections compared to MCNP reaction rates.

Key Words: SCALE, method of characteristics, CENTRM, continuous-energy transport calculation, self-shielded cross sections

1. INTRODUCTION

SCALE 6 [1] computes problem-dependent multigroup (MG) cross sections through a combination of the conventional Bondarenko shielding-factor method and a deterministic pointwise (PW) calculation of the fine-structure spectra in the resolved resonance and thermal energy ranges. BONAMI is a module of the SCALE system that is used to perform Bondarenko calculations for resonance self-shielding. Cross sections and Bondarenko factor data are input from an AMPX master library [2]. A wide variety of options are provided for different lattices and cell geometries through the use of Dancoff approximations. CENTRM computes PW neutron spectra in zero- or one-dimensional (1-D) systems, by solving the Boltzmann transport equation using a combination of PW and MG nuclear data. Several calculational options are available, including 1-D discrete ordinates in slab, spherical, or cylindrical geometry; a simplified two-region solution; and zone-wise or homogenized infinite media. In SCALE, CENTRM is used mainly to calculate problem-specific fluxes on a fine energy mesh (30,000–70,000 points), which may be used to generate self-shielded MG cross sections for subsequent criticality or shielding analysis.

The PW fluxes computed by CENTRM are not exact because a 1-D model is used for the transport calculation. In the case of a lattice of fuel pins, a 1-D PW transport calculation can be performed using a Wigner-Seitz cylindrical model with white boundary condition to represent

each unique unit pin cell. PW flux spectra calculated for the fuel, clad, moderator, etc., are used to process fine-group (e.g., 238 groups) cross sections for each component. These self-shielded cross sections are to be used in multidimensional deterministic or Monte Carlo transport calculations that explicitly represent the rectangular or hexagonal cell geometries, which results in a reactivity difference due to the geometrical effect on the self-shielded cross sections. Quantitative analysis in Ref. [3] showed that the effect of the geometrical inconsistency on the effective resonance cross sections is not negligible and that the amount of reactivity difference increases as dilution decreases in which dilution is a measure of self-shielding effect (e.g., infinite dilution means no self-shielding.). In order to solve this problem, the method of characteristics (MOC) has been implemented in CENTRM to perform MG and PW transport calculations to obtain accurate self-shielded cross sections within the exact 2-D cell geometry.

Resonance self-shielding methodologies in SCALE 6 are summarized in Section 2.1 and the MOC theory is described in Section 2.2. In Sections 3.1and 3.2, sample problems are provided and quantitative analyses for the geometrical and boundary condition effects on the self-shielded cross sections are performed by using the MCNP [4] and SCALE computational results.

2. METHODOLOGY

2.1. Resonance Self-Shielding Methodologies in SCALE 6

A flowchart of the SCALE modules executed for self-shielding is shown in Figure 1. [5] First, the fast-executing Bondarenko method is applied to all energy groups for the total, elastic, capture, and fission cross sections of all materials by using BONAMI. In this method MG data at problem-specific conditions are interpolated from the tabulated self-shielding factors in the MG library. While the analytical flux expression used to process Bondarenko shielding factors is reasonable for higher energy groups, it tends to break down at lower energies. SCALE 6 provides other approaches to generate problem-dependent MG data directly from PW data within the energy range in which the Bondarenko method is not desirable - typically the resolved resonance and thermal ranges for criticality safety and reactor physics applications. As shown in Figure 2, the energy range of interest is divided into the upper multigroup (UMR), PW, and lower multigroup (LMR) ranges, as defined by the input energy boundaries E_{max} and E_{min}, which have default values of 20 keV and 10^{-3} eV, respectively, in SCALE 6. Generally it is recommended that the PW energy range should encompass the resolved resonance ranges of all nuclides that impact the spectral fine-structure; however MG data in the UMR and LMR are always self-shielded with the Bondarenko method. Thus it is not necessary to perform a PW calculation within the energy range where the Bondarenko approximation is adequate. This is done by the CENTRM code, which computes neutron spectra on a fine energy mesh within the PW energy range using various approximations to the Boltzmann equation. In the energy region outside the specified PW range, CENTRM performs an MG calculation so that a full energy range solution is obtained.

The PMC module computes problem-specific MG data for groups within the PW energy range of the CENTRM calculation and replaces the more approximate values from BONAMI. PMC uses the CENTRM spectra for each spatial region as a *problem-dependent weight function* for averaging energy-dependent data in the PW libraries into MG data. The resulting problem-

specific cross-section library is passed to higher-dimensional MG transport calculations performed with other SCALE modules.

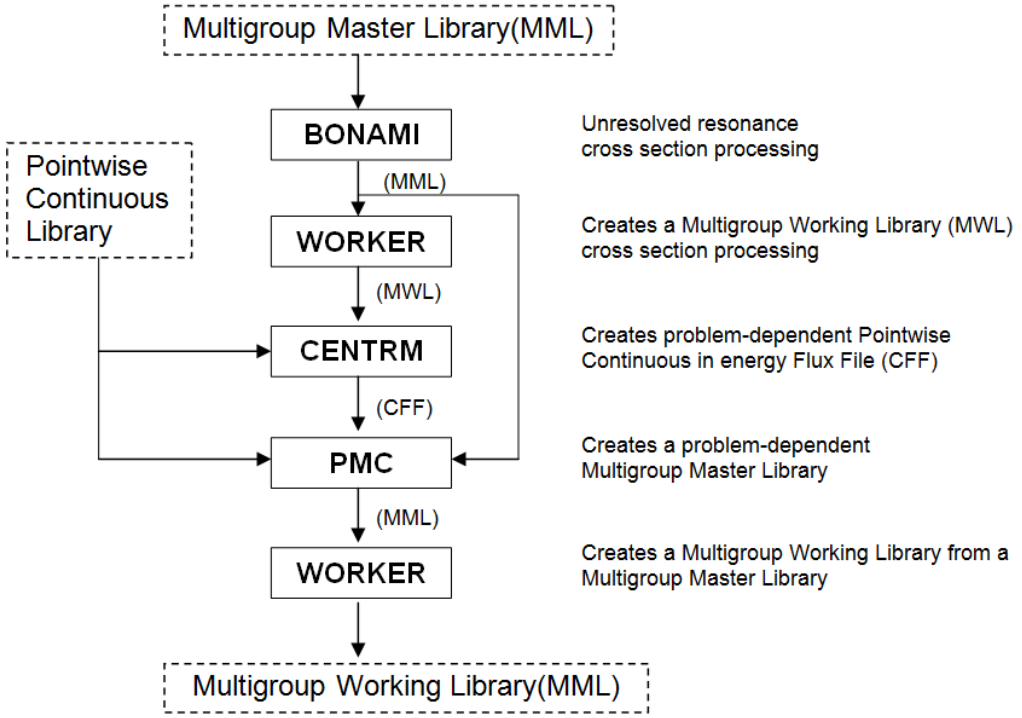

Figure 1. Flowchart of modules used to generate problem-dependent multigroup data.

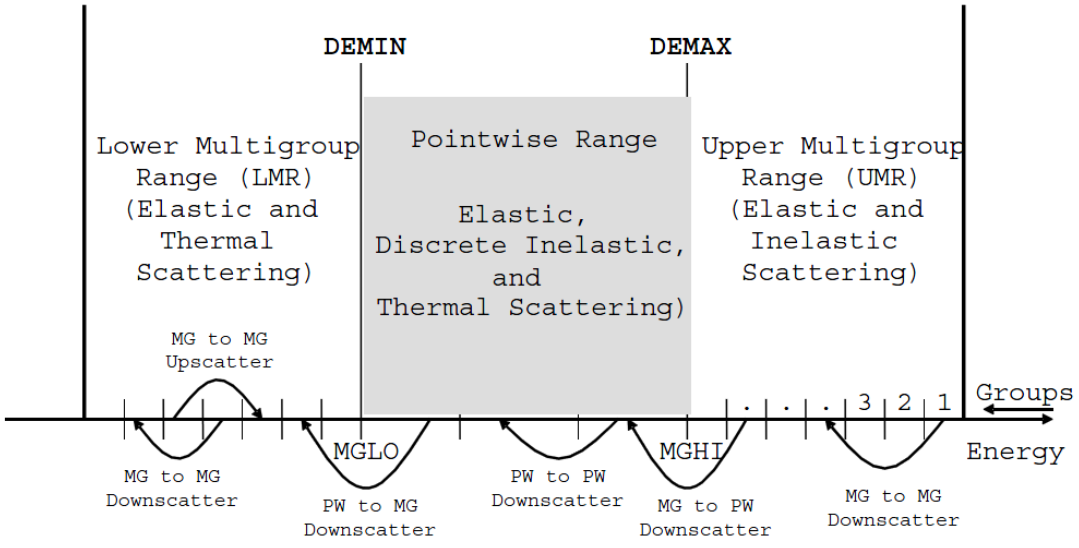

Figure 2. Definition of UMR, PW, and LMR energy ranges.

2.2. The Method of Characteristics

The MOC [6, 7, 8] adopts the advantages of the integral transport method and the discrete ordinate method (S_N). The former is better in treating a complex geometry, and the latter is better in treating anisotropic scattering problems and does not require a full collision probability matrix. The MOC is used for the spatial discretization, which is primarily an approximation for the streaming plus collision operator on the left side of the transport equation.

Figure 3 shows the characteristics lines in the direction of $\hat{\Omega}_m$ for a rectangular mesh cell where the line spacing does not have to be equal. However, the equal line spacing is recommended to make the problem treatment and implementation easy and simple in practice. Although the direction $\hat{\Omega}_m$ and the track length s_{mik} in mesh cell i along track k are represented in an x-y plane in Figure 3, they are three-dimensional quantities in reality. The rays passing through a mesh cell define specific tracks of width δA_m and length s_{mik}; the angular flux of each track is representative of the flux in the volume $s_{mik}\,\delta A_m$. If there are an infinite number of tracks in a mesh cell, the quadrature summation will be same as the analytic integration. However, since we have a finite number of ray tracks in reality, there must be some difference between the quadrature summation and the integration. Each track s_{mik} should be adjusted to conserve mesh cell volume. If the incident angular fluxes and source Q are known, the outgoing angular fluxes along the characteristics line can be obtained by using Eq. (1).

$$\psi_{mik}(s_{mik}) = \psi_{mik}(0)e^{-\Sigma_i s_{mik}} + \frac{1}{4\pi}\frac{Q_i}{\Sigma_i}\left[1 - e^{-\Sigma_i s_{mik}}\right], \tag{1}$$

where Σ_i denotes the total macroscopic cross section and the ray incidence position is taken as zero.

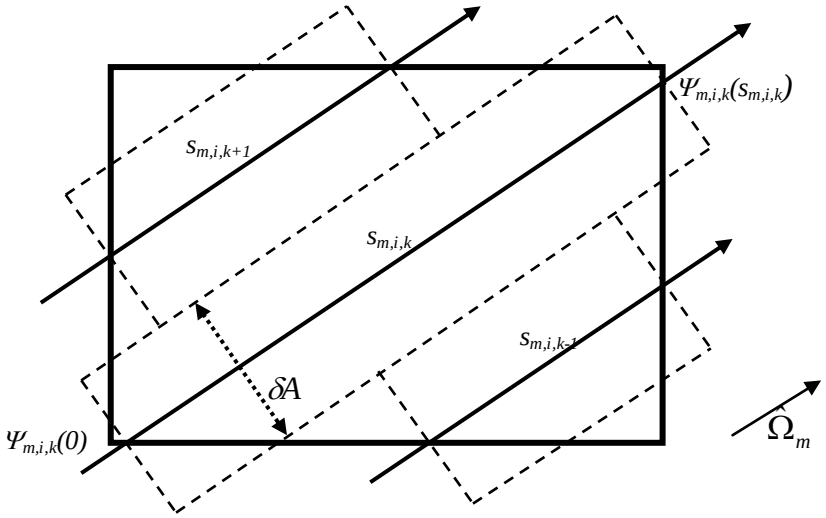

Figure 3. Tracks passing through cell *i* in the characteristic direction $\hat{\Omega}_m$.

The MOC assumes that within each mesh cell both the material properties and the source are constant. These assumptions allow the exact evaluation of the integral terms in Eq. (1) to obtain the exiting angular flux for each track passing through mesh cell *i*. The average angular flux in each track can be computed as follows:

$$\overline{\psi}_{mik} = \frac{1}{s_{mik}} \int_0^{s_{mik}} ds' \psi_{mik}(s') = \frac{\psi_{mik}(0) - \psi_{mik}(s_{mik})}{\Sigma_i s_{mik}} + \frac{1}{4\pi} \frac{Q_i}{\Sigma_i}. \quad (2)$$

Within each track s_{mik}, $\overline{\psi}_{mik}$ is the average angular flux in mesh cell *i* along track *k* in the characteristic direction $\hat{\Omega}_m$. The average angular flux in the mesh cell *i* is computed as the volume-weighted average of all tracks crossing the mesh cell,

$$\overline{\psi}_{mi} = \frac{\sum_{k \in i} \overline{\psi}_{mik} s_{mik} \delta A_m}{\sum_{k \in i} s_{mik} \delta A_m}. \quad (3)$$

From the discrete ordinates approximation, the scalar flux in each mesh cell is simply the sum over all ordinates of the average angular flux:

$$\phi_i = \sum_{m=1}^{M} w_m \overline{\psi}_{mi} = \sum_{m=1}^{M} w_m \frac{\sum_{k \in i} \overline{\psi}_{mik} s_{mik} \delta A_m}{\sum_{k \in i} s_{mik} \delta A_m}. \quad (4)$$

In order to save computing time, a 1/8 symmetry pin cell model has been utilized. Azimuthal angles and ray spacings are determined to have a perfect reflection at the boundaries for 1/4 symmetry pin cell model. A perfect reflection means that the boundary position and reflected angle of an exiting ray should meet exactly with those of one of the incident rays. A quarter symmetry model with a perfect reflection guarantees a perfect reflection for 1/8 symmetry pin cell model.

3. CALCULATION AND RESULTS

3.1 Sample Problems

Three sample problems have been selected for typical fuel pins of a pressurized water reactor (PWR). In order to consider various dilutions, three different configurations were used in which the second one is for the typical PWR pin, the first one for low dilution and the last one for high dilution. The CENTRM calculations were performed for these sample problems by using the S_N and MOC methods for Wigner-Seitz cylindrical and square pin configurations, respectively, shown in Figure 4. The reference solutions were obtained by performing three MCNP calculations for the square pin configurations in which reflecting boundary conditions were imposed. The MCNP calculations used CE cross-section libraries based on ENDF/B-VII processed by NJOY [9], and the SCALE MG calculations used ENDF/B-VII CE data and 238-

group SCALE library processed by the AMPX code package. Geometry and composition data for the sample problems are shown in Table I.

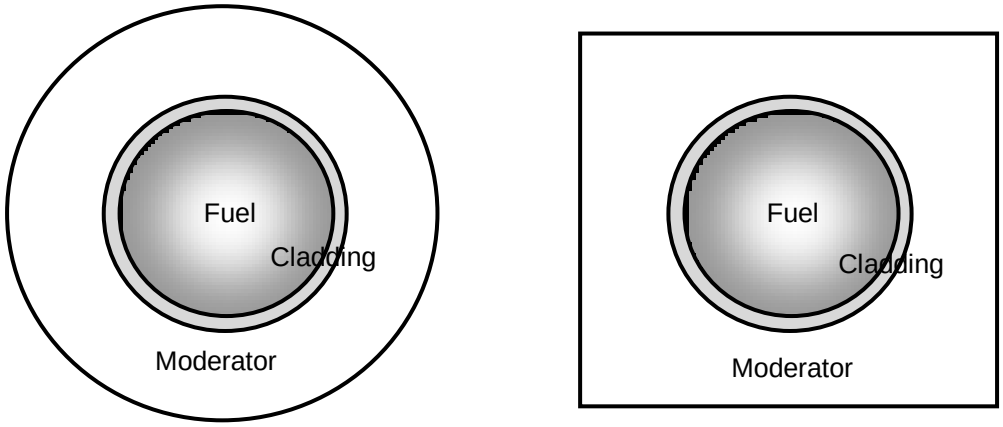

Figure 4. Wigner-Seitz cylindrical and square pin cell models.

Table I. Geometry and composition

Region		Material	Temperature (K)	Radius (pitch) (cm)	Density (g/cm^3)
Fuel		UO_2	600	0.4025	10.4
Clad		^{27}Al	600	0.4759	2.7
Moderator	**Case A**	H_2O	600	0.7120 (1.2620)	0.13
	Case B			0.7120 (1.2620)	0.65
	Case C			1.2762 (2.2621)	0.65

Figure 5 provides normalized neutron spectra per lethargy as a function of neutron energy for the three different pin configurations, which were obtained by MCNP reference calculations. While neutron spectrum for Case A is very hardened due to an 80% void in the water moderator, the neutron spectrum for Case C is softened due to over-moderation caused by the larger moderator-to-fuel volume ratio.

MG scalar fluxes, microscopic absorption, fission, and elastic scattering cross sections and the number of neutrons released per fission were edited for ^{235}U and ^{238}U with the 238-group SCALE energy structure from the MCNP and BONAMI/CENTRM/PMC calculations. The CENTRM calculations were performed for the Wigner-Seitz cylindrical pin model by using the S_N method and for the square pin model by using MOC. The CENTRM-S_N calculations utilized an S6 quadrature order, 15 upscatter outer iterations in the thermal range, 12 spatial intervals, and P_1 scattering order. The CENTRM-MOC calculations used three polar and eight azimuthal angles per quadrant, 0.02 cm ray spacing, one flat source region per each material zone, and P_0 scattering order. The MCNP results should provide accurate self-shielded resonance cross sections. The total number of neutron histories for the MCNP calculations was 300 million, and

inactive and active cycles were 50 and 100, respectively. The CENTRM calculations were performed for all three cases with the S_N method for the circular pin configuration with white boundary condition and the MOC method for the square pin configuration with reflecting boundary condition, respectively. Minimum and maximum energies for the pointwise transport calculation were set to 0.0001 eV and 400 keV, respectively.

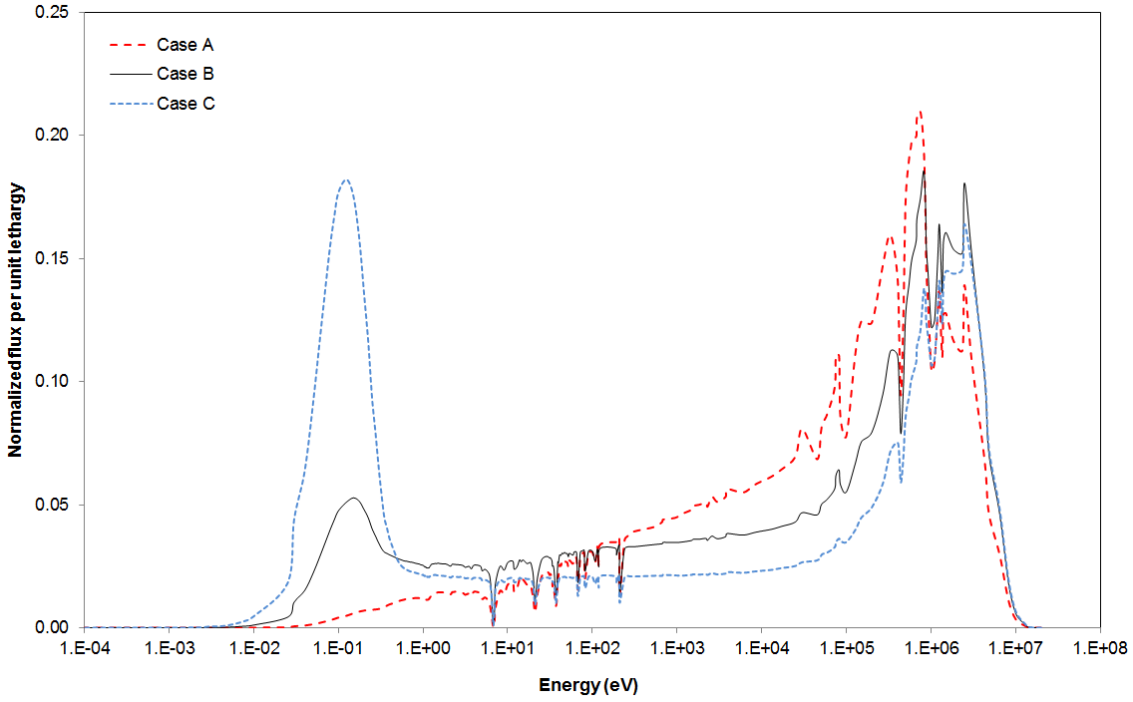

Figure 5. Neutron spectra for sample problems.

3.2 Results and Analysis

Figure 6 provides a comparison of 238-group cross sections generated by the BONAMI/ CENTRM-S_N calculations with those generated by the MCNP calculations for Case B. Although there are some differences in the MG cross sections, it is more important to compare reaction rates. If the differences result in a negligible effect on the multiplication factor, then the MG cross sections can be used in the subsequent transport lattice codes without causing any significant discrepancy in various nuclear parameters. In order to show the effects of the cross-section differences on reactivity, the reactivity differences due to the cross-section differences were estimated for each group. The following relationships were used for analysis the same scalar fluxes were used for both cases so that only the impact of the cross section differences was treated.

$$k_{inf} = \frac{\sum_i \sum_{g'} N_i \nu \sigma_{f,g',i} \phi_{g'}}{\sum_i \sum_{g'} N_i \sigma_{a,g',i} \phi_{g'}}, \tag{5}$$

$$\Delta\rho_{a,g} = \left(\frac{\sum_i \sum_{g'} N_i \sigma_{a,g',i} \phi_{g'} - \sum_i N_i \sigma_{a,g,i} \phi_g}{\sum_i \sum_{g'} N_i \nu \sigma_{f,g',i} \phi_{g'}} - \frac{1}{k_{inf}} \right) \cdot 10^5, \tag{6}$$

$$\Delta\rho_{\nu f,g} = \left(\frac{\sum_i \sum_{g'} N_i \sigma_{a,g',i} \phi_{g'}}{\sum_i \sum_{g'} N_i \nu \sigma_{f,g',i} \phi_{g'} - \sum_i N_i \nu \sigma_{f,g,i} \phi_g} - \frac{1}{k_{inf}} \right) \cdot 10^5, \tag{7}$$

and

$$\Delta\rho_g = \sum_g (\Delta\rho_{a,g}^{MCNP} - \Delta\rho_{a,g}^{SCALE} + \Delta\rho_{\nu f,g}^{MCNP} - \Delta\rho_{\nu f,g}^{SCALE}), \tag{8}$$

where *i* denotes nuclide, *g* denotes energy group, N_i is the atomic number density, k_{inf} is the infinite multiplication factor, ν is the number of neutrons released per fission, $\sigma_{f,g,i}$ is the fission cross section, $\sigma_{a,g,i}$ is the absorption cross sections, and ϕ_g is the MCNP scalar flux.

Figures 7–9 provide a comparison of reactivity differences between MCNP and BONAMI/ CENTRM-S_N for Cases A, B, and C, which were obtained by using Eqs. (5–8). The whole energy range is divided into three broad groups, called thermal, epithermal, and fast. Their boundaries are 0.0–0.625 eV, 0.625–13,000 eV and 13,000 eV–20 MeV, respectively. The 238-group reactivity differences between MCNP and BONAMI/ CENTRM-S_N are merged into three broad groups and are shown in Table II. When Figure 6 is compared to Figure 8, the shape of cross section difference is very different from that of reactivity differences. While Figure 7 (Case A at low dilution) shows large reactivity differences, Figure 9 (Case C at high dilution) shows only slight reactivity differences. As the dilution decreases, the reactivity differences increase significantly. At very high dilution , there are almost no reactivity differences which physically means that the boundary condition and shape do not significantly impact on self-shielding. For the nominal fuel pin (Case B), there are only slight differences at the thermal and fast energy groups, which can be negligible when considering the statistical uncertainty in MCNP. However, there is a 185 pcm reactivity difference between MCNP and SCALE with CENTRM-S_N for the epithermal energy group. Reactivity differences for Cases A and B mostly come from discrepancies in the self-shielded cross sections, which implies that the boundary condition and shape at low dilution has a significant impact on the self-shielding effect.

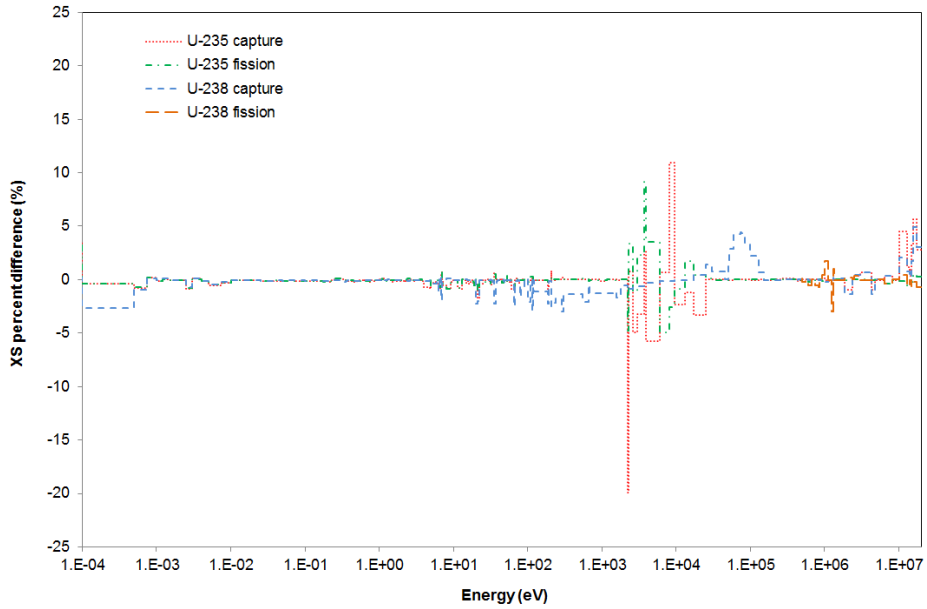

Figure 6. Cross section differences between MCNP and BONAMI/CENTRM-S_N (Case B).

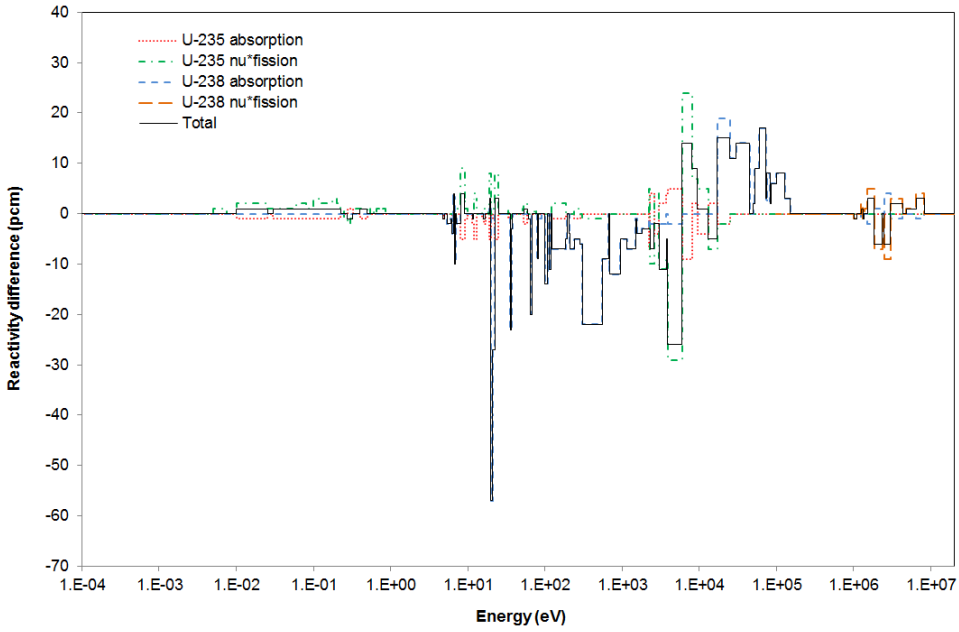

Figure 7. Reactivity differences due to the cross-section differences between MCNP and BONAMI/CENTRM-S_N (Case A).

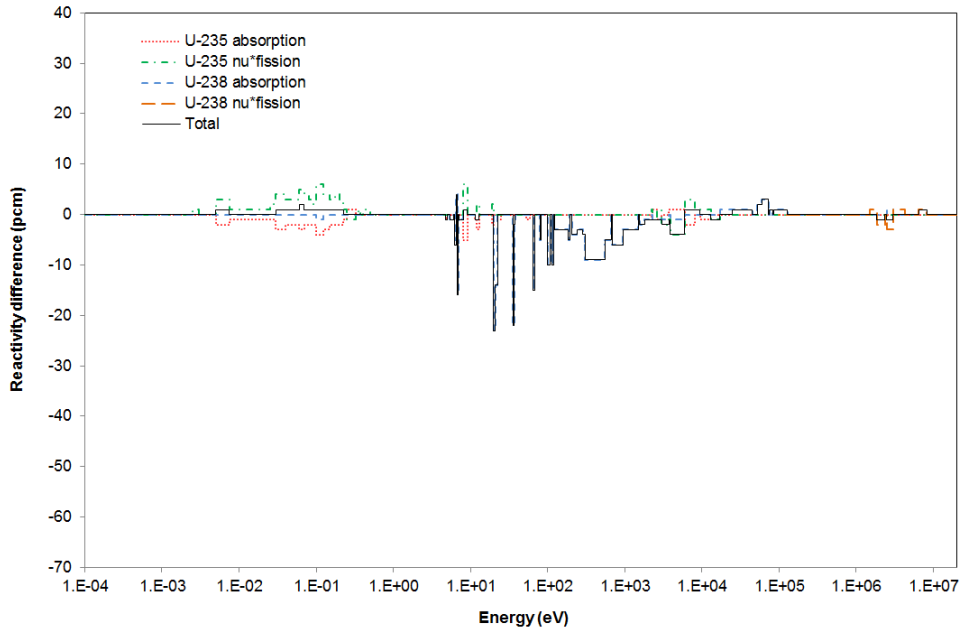

Figure 8. Reactivity differences due to the cross-section differences between MCNP and BONAMI/CENTRM-S_N (Case B).

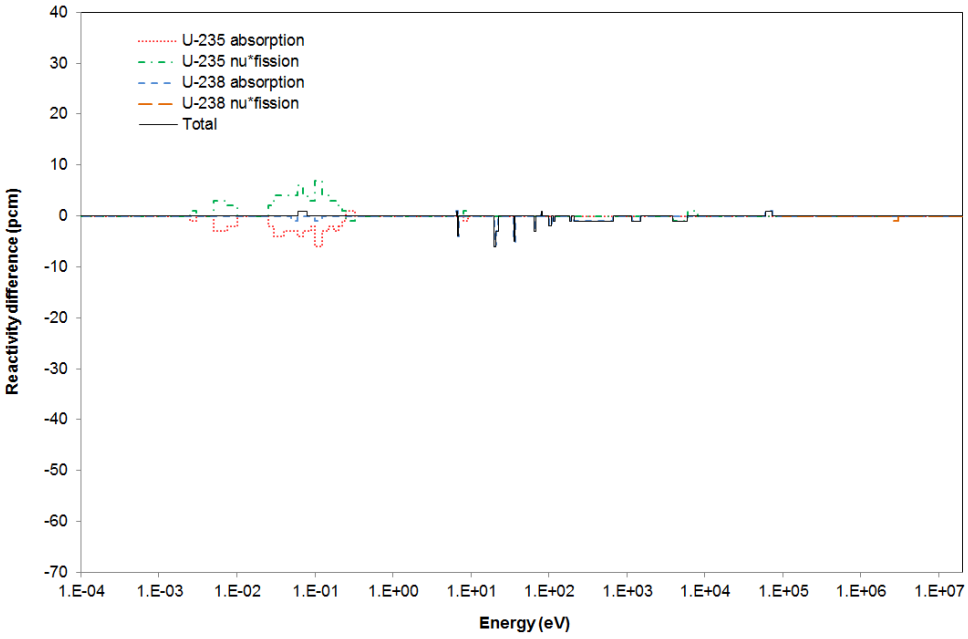

Figure 9. Reactivity differences due to the cross-section differences between MCNP and BONAMI/CENTRM-S_N (Case C).

Table II. Reactivity differences for each broad group between MCNP and BONAMI/CENTRM-S_N (unit: pcm)

Case	Group	^{235}U		^{238}U		Total
		absorption	ν*fission	absorption	ν*fission	
A	Fast[a]	0	-8	102	-3	91
	Epithermal[b]	-45	33	-287	0	-300
	Thermal[c]	-13	27	-2	0	12
	Sum	-58	52	-187	-3	-197
B	Fast	0	-1	14	-2	11
	Epithermal	-20	14	-179	0	-185
	Thermal	-35	51	-4	0	12
	Sum	-55	64	-168	-2	-161
C	Fast	0	0	3	-1	2
	Epithermal	-2	1	-30	0	-31
	Thermal	-45	55	-5	0	5
	Sum	-48	56	-31	-1	-24

[a] 13.0 keV ~ 20.0 MeV
[b] 0.625 eV ~ 13.0 keV
[c] 0.0 eV ~ 0.625 eV

Figures 10–12 provide comparisons of reactivity differences between MCNP and BONAMI/CENTRM-MOC for Cases A, B, and C, and the broad group reactivity differences are summarized in Table III. When Figure 10 and Table III for Case A are compared to Figure 7 and Table II, there are almost no changes for the thermal and fast groups. However, there is about a 180 pcm improvement at the epithermal energy group. As shown in Figure 10, there are some reactivity differences at the epithermal energy groups. When Figure 11 and Table III for Case B are compared to Figure 8 and Table II, there is a significant improvement in the reactivity differences at the epithermal energy group. When considering the statistical uncertainty, there is almost no difference in the reactivities for all nuclide reaction rates. The total reactivity difference for the typical PWR pin cell between MCNP and BONAMI/CENTRM-MOC is only 26 pcm. The BONAMI/CENTRM-MOC procedure is able to provide very precise self-shielded cross sections for the following SCALE multidimensional transport calculations.

Although significant improvements are shown by using an explicit 2-D geometry and boundary condition treatment, it should be noted that there are still reactivity differences for low dilution problems. Since nuclear fuel with a very hardened neutron spectrum includes more anisotropic characteristics in neutron behavior, it is probable that these discrepancies may be attributed to the order of neutron scattering. The discrepancies should be determined in the near future to apply the CENTRM procedure to the fuel configuration with a very hardened neutron spectrum.

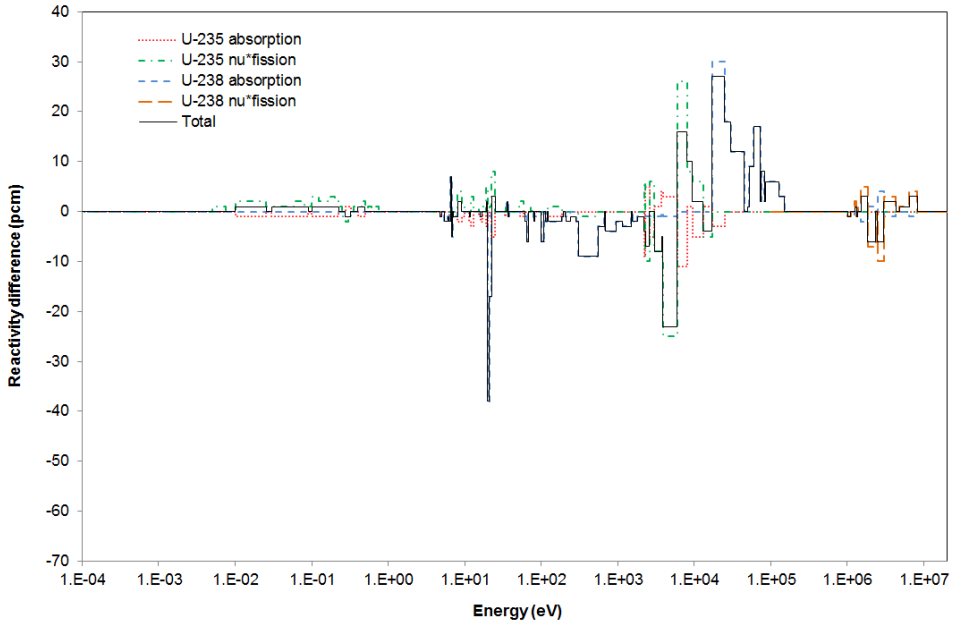

Figure 10. Reactivity differences due to the cross-section differences between MCNP and BONAMI/CENTRM-MOC (Case A).

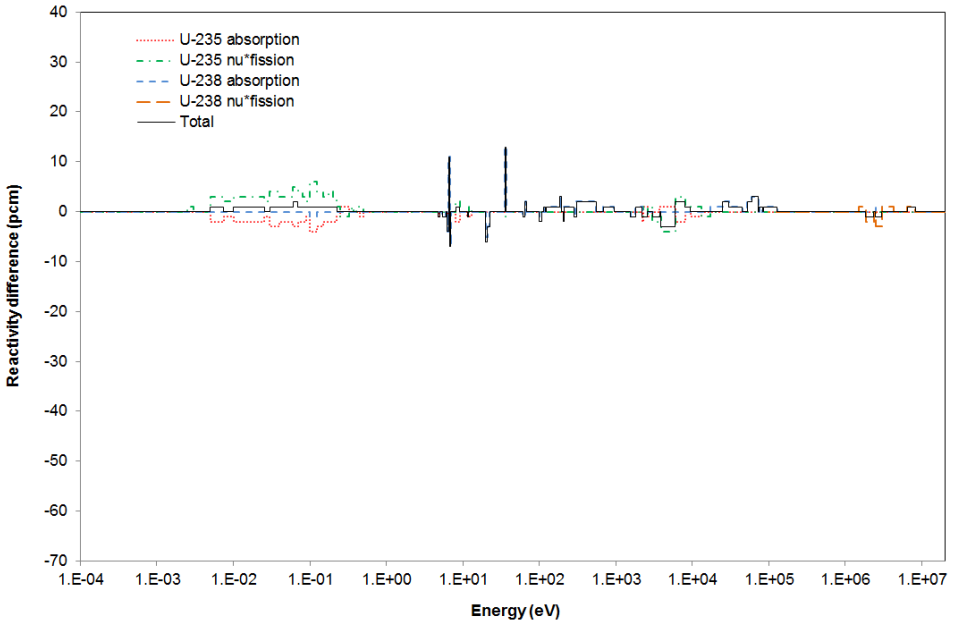

Figure 11. Reactivity differences due to the cross-section differences between MCNP and BONAMI/CENTRM-MOC (Case B).

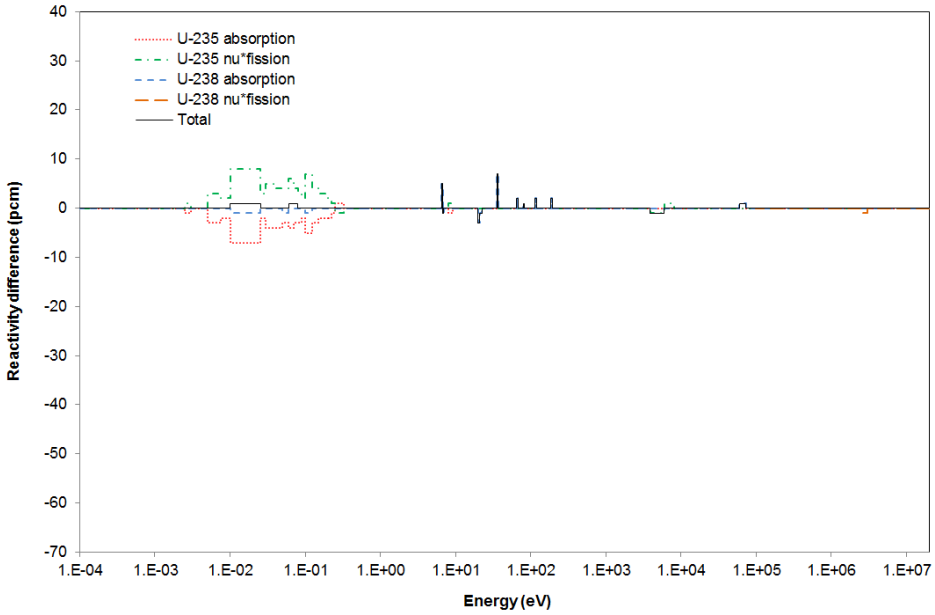

Figure 12. Reactivity differences due to the cross-section differences between MCNP and BONAMI/CENTRM-MOC (Case C).

Table III. Reactivity differences for each broad group between MCNP and BONAMI/CENTRM-MOC (unit: pcm)

Case	Group	^{235}U		^{238}U		Total
		absorption	ν*fission	absorption	ν*fission	
A	Fast[a]	-2	-5	114	-3	104
	Epithermal[b]	-45	33	-114	0	-126
	Thermal[c]	-13	28	-2	0	13
	Sum	-60	56	-2	-3	-10
B	Fast	0	-1	14	-2	11
	Epithermal	-9	3	8	0	2
	Thermal	-37	53	-4	0	13
	Sum	-45	55	19	-2	26
C	Fast	0	0	3	-1	2
	Epithermal	-1	0	14	0	13
	Thermal	-53	63	-5	0	5
	Sum	-54	63	11	-1	20

[a] 13.0 keV ~ 20.0 MeV
[b] 0.625 eV ~ 13.0 keV
[c] 0.0 eV ~ 0.625 eV

3. CONCLUSIONS

Typically self-shielded cross sections in the resolved resonance energy range are generated by performing pointwise transport calculations defined on an ultra-fine energy grid for 1-D cylindrical pin cells. These self-shielded cross sections are used in a transport lattice calculation for arrays of rectangular or hexagonal pin cells, which results in a reactivity difference due to the geometrical effect on generating the self-shielded cross sections. Quantitative analysis shows that the effect of the geometrical inconsistency on the self-shielded cross sections is not negligible and the amount of reactivity difference increases as dilution decreases. The method of characteristics has been applied to performing pointwise transport calculations to estimate the self-shielded cross sections for square pin cells to avoid the geometrical approximation and to improve the numerical accuracy. The computational results show that the pointwise transport calculations with 2-D MOC without any geometrical approximation generate more accurate self-shielded cross sections than the 1-D cylindrical Wigner-Seitz S_N model.

Although a significant improvement has been made through the MOC implementation into CENTRM, still there is a discrepancy in reaction rates at very low dilution. This discrepancy remains under investigation.

ACKNOWLEDGMENTS

The work presented here was sponsored by the U.S. Nuclear Regulatory Commission Office of Research.

REFERENCES

1. *SCALE: A Modular Code System for Performing Standardized Computer Analyses for Licensing Evaluation*, ORNL-TM/2005/39, Version 6, Vols. I–III, Oak Ridge National Laboratory, Oak Ridge, Tenn. (2009). (Available from Radiation Safety Information Computational Center at Oak Ridge National Laboratory as CCC-750.)
2. M. E. Dunn and N. M. Greene, "AMPX-2000: A Cross-Section Processing System for Generating Nuclear Data for Criticality Safety Applications," *Trans. Am. Nucl. Soc*. **86**, 118–119 (2002).
3. Kang-Seog Kim and Ser Gi Hong, "The Method of Characteristics Applied to Solving Slowing Down Equation to Estimate the Self-Shielded Resonance Cross Sections with an Explicit Geometrical Effect," *Ann. Nucl. Energ*., **38**, 438-446 (2011).
4. J.F. Breismeister, et al., "MCNP – A General Monte Carlo N-Particle Transport Code Version 4B," LA-12625-M (1997).
5. Mark L. Williams, "Resonance Self-Shielding Methodologies in SCALE 6," *Nuclear Technology*, **174**, 149-168 (2011).
6. J.R. Askew, "The Current UK Position on Uranium-238 Resonance Capture," *Seminar on ^{238}U Resonance Capture Held at National Neutron Cross Section Center*, Brookhaven National Laboratory Upton, New York, USA, March 18-20, 1975, BNL-NCS-50451 (ENDF-217) (1975).

7. M.R. Wagner, et al., "A Numerical Method for the Solution of Three-Dimensional Neutron Transport Problems," *Nucl. Sci. Eng.*, **41**, 14 (1970).
8. K. Takeuchi, "Numerical Solution to the Space-Angle Energy Dependent Neutron Integral Transport Equation," *J. Nucl. Sci. Tech.*, **8**, 141 (1971).
9. R.E. MacFarlane, D.W. Muir, "The NJOY Nuclear Data Processing System Version 91," LA-12740-M Manual (1994).